DEVELOPMENT OF LEAD-FREE TUNGSTEN CARBIDE-BASED POLYMERIC BRICKS AS GAMMA RADIATION SHIELDING

NADIN J D ABUALROOS

UNIVERSITI SAINS MALAYSIA

2022

DEVELOPMENT OF LEAD-FREE TUNGSTEN CARBIDE-BASED POLYMERIC BRICKS AS GAMMA RADIATION SHIELDING

by

NADIN J D ABUALROOS

Thesis submitted in fulfilment of the requirements
for the degree of
Doctor of Philosophy

June 2022

ACKNOWLEDGEMENT

First and foremost, all gratitude and praise to Allah the almighty, who gave me the strength to fight in this life even in the most difficult times Allah was beside me and he will always be. I am expressing all thanks to Allah the Almighty and Merciful for granting me the strength to complete this work.

I would like to express immense gratitude to my main supervisor Associate Professor Dr Rafidah Zainon for all the support and advice, for all the great discussions, the new knowledge and guidance. My sincere appreciation for my co-supervisor Associate. Professor Dr Haidi bin Ibrahim for his support throughout the study.

I also would like to thank Advanced Medical and Dental Institute staff for providing a great environment and facilities to all students. Special thanks to nuclear medicine department staff particularly Mr. Khairul Nizam Jaafar for his great technical assistance.

Special thanks to the laboratories staff who provided me with their valuable assistance in the Advanced Medical and Dental institute, School of Physics, School of Archelogy, Science and Engineering Research Centre at USM, and School of Nuclear Sciences at UKM. In addition, I would like to thank Universiti Sains Malaysia for their financial assistance in granting me the USM fellowship for two years during this research work.

To the strongest, most caring, most special, and beautiful people in my life my parents, my dad Jamal Daoud Abualroos and my mom Imtiaz Hassan Abualroos, thank you mom and dad for all the love you give to me, for always being there for me, thanks for keep believing in me and being my all-time supporters. Thank you from the bottom of my heart for your great unconditional love and sacrifices. I am

everything I am because of you. To my soulmates and the apple of my eyes Heba, Mohammed and shareef thank you for being the best family and the most wonderful siblings in the world. To my nephews Yousef, Essa, and Yazan. I dedicate this thesis to them.

Finally, I extend my deepest regards and blessings to all those, who supported me in any aspect during the completion of this research and to my friends for all the encouragement and the great memories.

TABLE OF CONTENTS

ACKNOWLEDGEMENT ..... **ii**

TABLE OF CONTENTS ..... **iv**

LIST OF TABLES ..... **x**

LIST OF FIGURES ..... **xiii**

LIST OF SYMBOLS ..... **xxii**

LIST OF ABBREVIATIONS ..... **xxiv**

LIST OF APPENDICES ..... **xxvi**

ABSTRAK ..... **xxvii**

ABSTRACT ..... **xxix**

CHAPTER 1 INTRODUCTION **1**

1.1 Background 1

1.2 Problem statement 6

1.3 Research objectives 9

1.4 Scope of the study 10

1.5 Structure of the study 11

CHAPTER 2 LITERATURE REVIEW **13**

2.1 Introduction 13

2.2 Ionising radiation 13

2.2.1 Production of gamma rays 14

2.3 Radiation interaction with matter 17

2.3.1 Photoelectric effect 17

2.3.2 Compton scatter 18

2.3.3 Pair production 19

2.4 Gamma ray attenuation 21

2.4.1 Linear attenuation coefficient 22

2.4.2 Mass attenuation coefficient 24
2.4.3 Mean free path 26
2.4.4 Half value layer and tenth value layer 27
2.4.5 Radiation protection efficiency (RPE) 27
2.5 Biological effects of radiation exposure 27
2.6 Radiation shielding: concept and practice 29
2.7 Lead as conventional radiation shielding material 31
2.7.1 Lead properties and applications 31
2.7.2 Lead substitution 31
2.7.3 Health hazards associated with lead shielding 34
2.7.3(a) Immune system 34
2.7.3(b) Reproductive system 35
2.7.3(c) Renal system 35
2.7.3(d) Nervous system 35
2.7.4 Development of new lead-free radiation shielding materials 36
2.8 Polymer composites radiation shielding material 37
2.9 Potential radiation shielding materials 38
2.9.1 Tungsten carbide and tungsten carbide cobalt 38
2.9.2 Barium sulphate and bismuth oxide as additives materials 40
2.9.3 Epoxy resin as binder 42
CHAPTER 3 MATERIALS AND METHODOLOGY 43
3.1 Introduction 43
3.2 Materials 43
3.2.1 Tungsten carbide 43
3.2.2 Tungsten carbide cobalt 44
3.2.3 Bismuth oxide 45
3.2.4 Barium sulphate 46

3.2.5 Epoxy resin and hardener 46

3.3 Experimental Flow Chart 47

3.3.1 Sample preparations 49

3.3.1(a) Preparation of tungsten carbide-based epoxy resin composites 49

3.3.1(b) Brick fabrication 54

3.4 Characterisation equipment for radiation shielding materials 55

3.4.1 Field emission scanning electron microscopy (FESEM)/ Energy dispersive X-ray spectroscopy (EDX) 55

3.4.2 Fourier transform infrared spectroscopy (FTIR) 63

3.4.3 Gamma spectroscopy 66

3.4.4 Single photon emission computed tomography (SPECT) 72

3.4.5 Vickers hardness tester 76

3.5 Physical, mechanical, and radiation shielding properties of the fabricated composites 80

3.5.1 Physical properties 80

3.5.1(a) Density measurements 80

3.5.1(b) Effective atomic number (Z_{eff}) 80

3.5.2 Mechanical properties 81

3.5.3 Radiation shielding properties 82

3.6 Statistical analysis 82

CHAPTER 4 RESULTS AND DISCUSSION 84

4.1 Introduction 84

4.2 Tungsten carbide epoxy resin brick 84

4.3 Density measurements 89

4.4 Elemental compositions and effective atomic number 93

4.4.1 Elemental compositions 93

4.4.1(a) EDX measurements of epoxy resin 93

4.4.1(b) EDX measurements of tungsten carbide powder and tungsten carbide-based epoxy resin composites 94

4.4.1(c) EDX measurements of tungsten carbide cobalt powder and tungsten carbide cobalt-based epoxy resin composites 94

4.4.1(d) EDX measurements of barium sulphate powder and tungsten carbide barium sulphate-based epoxy resin composites 95

4.4.1(e) EDX measurements of bismuth oxide and tungsten carbide bismuth oxide-based epoxy resin composites 96

4.4.2 Effective atomic number (Z_{eff}) 97

4.5 Morphological properties 99

4.5.1 FESEM - morphological features of neat epoxy resin 99

4.5.2 FESEM - morphological features of tungsten carbide (WC) powder 100

4.5.3 FESEM - morphological features of tungsten carbide cobalt (WC-Co) powder 101

4.5.4 FESEM - morphological features of barium sulphate ($BaSO_4$) powder 102

4.5.5 FESEM - morphological features of bismuth oxide (Bi_2O_3) powder 103

4.5.6 FESEM - morphological features of tungsten carbide-based epoxy resin composites 104

4.5.7 FESEM - morphological features of tungsten carbide cobalt-based epoxy resin composites 106

4.5.8 FESEM - morphological features of tungsten carbide barium sulphate-based epoxy resin composites 107

4.5.9 FESEM - morphological features of tungsten carbide bismuth oxide-based epoxy resin composites 108

4.6 Mechanical properties 109

4.7 Chemical properties 112

4.8 Attenuation measurements 116

4.8.1 Energy calibration of the spectrometer 116

4.8.2 Attenuation coefficient measurements 120

4.8.2(a) Attenuation measurements of the fabricated samples with 40% epoxy resin 121

4.8.2(b) Attenuation measurements of the fabricated samples with 35% epoxy resin 123

4.8.2(c) Attenuation measurements of the fabricated samples with 30% epoxy resin 125

4.8.2(d) Attenuation measurements of the fabricated samples with 25% epoxy resin 127

4.8.2(e) Attenuation measurements of the fabricated samples with 20% epoxy resin 130

4.8.2(f) Attenuation measurements of the fabricated samples with 15% epoxy resin 132

4.8.2(g) Attenuation measurements of the fabricated samples with 10% epoxy resin 134

4.8.2(h) Attenuation coefficients obtained by XCOM of the fabricated samples with 10% and 15% epoxy resin 138

4.8.3 Half value layer (HVL), tenth value layer (TVL) and mean free path (MFP) 141

4.8.3(a) Fabricated samples with 15% epoxy resin..... 141

4.8.3(b) Fabricated samples with 10% epoxy resin..... 145

4.8.4 Radiation protection efficiency 148

4.8.4(a) Radiation protection efficiency of the fabricated samples with 15% epoxy resin 148

4.8.4(b) Radiation protection efficiency of the fabricated samples with 10% epoxy resin 149

4.9 Validation of the fabricated bricks 151

CHAPTER 5 CONCLUSION AND FUTURE RECOMMENDATIONS.... 156

5.1 Conclusion..... 156

5.2 Limitations of the study..... 158

5.3 Recommendations for future research..... 158

REFERENCES..... 159

APPENDICES

LIST OF PUBLICATIONS

LIST OF CONFERENCES

LIST OF INTELLECUAL PROPERTY

LIST OF TABLES

Page

Table 2.1 Atomic number and density of lead, tungsten and bismuth. 32

Table 3.1 General properties of tungsten carbide powder. 43

Table 3.2 General properties of tungsten carbide cobalt powder. 44

Table 3.3 General characteristics of bismuth oxide powder. 45

Table 3.4 General characteristics of barium sulphate powder. 46

Table 3.5 Physical, chemical, and mechanical properties of E-110I/H-9 epoxy resin. 47

Table 3.6 Different weight percentages of powder-epoxy resin composites. 49

Table 3.7 The list of prepared samples with different weight percentage of tungsten carbide and epoxy resin. 52

Table 3.8 The list of prepared samples with different weight percentage of tungsten carbide cobalt and epoxy resin. 52

Table 3.9 The list of prepared samples with different weight percentage of tungsten carbide, barium sulphate and epoxy resin. 53

Table 3.10 The list of prepared samples with different weight percentage of tungsten carbide, bismuth oxide and epoxy resin. 53

Table 3.11 List of the total number of the 16 final fabricated bricks. 54

Table 3.12 The samples characterised by using FESEM/EDX analysis test. 60

Table 3.13 Tungsten carbide epoxy composites samples for FESEM/EDX analysis test. 60

Table 3.14 Tungsten carbide cobalt epoxy composites samples for FESEM/EDX analysis test 61

Table 3.15 Tungsten carbide/barium sulphate/epoxy resin composites samples for FESEM/EDX analysis test. 62

Table 3.16 Tungsten carbide/bismuth oxide/epoxy resin composites samples for FESEM/EDX analysis test. 62

Table 3.17 Chemical and physical properties of the selected radiation point sources. 70

Table 3.18 Radionuclides used with their corresponding gamma-ray emission energies and initial activities. 75

Table 4.1 Density of the fabricated WCE and WCoE samples. 90

Table 4.2 Density of the fabricated WC-$BaSO_4$-E samples. 90

Table 4.3 Density of the fabricated WC-Bi_2O_3-E samples. 91

Table 4.4 Elemental composition of epoxy resin sample by weight and atomic percentages. 93

Table 4.5 Elemental composition of tungsten carbide powder. 94

Table 4.6 Elemental composition of tungsten carbide-based epoxy (WCE) samples by weight and atomic percentages. 94

Table 4.7 Elemental composition of tungsten carbide cobalt powder. 95

Table 4.8 Elemental composition of tungsten carbide cobalt-based epoxy resin sample with weight and atomic percentages. 95

Table 4.9 Elemental composition of barium sulphate powder. 96

Table 4.10 Elemental composition of tungsten carbide barium sulphate-based epoxy resin samples by weight and atomic percentages. 96

Table 4.11 Elemental composition of bismuth oxide powder. 96

Table 4.12 Elemental composition of tungsten carbide-based bismuth oxide epoxy resin samples with atomic and weight percentages. 97

Table 4.13 Vickers hardness values of the investigated samples. 109

Table 4.14 Measurement data of Gamma Reference Sources. 116

Table 4.15 Gamma ray sources with their corresponding energies. 117

Table 4.16 LAC and MAC of the fabricated samples with 0.7 cm and 1.4 cm thickness and 40% weight epoxy resin. 121

Table 4.17 LAC and MAC of the fabricated samples with 0.7 cm and 1.4 cm thickness and 35% weight epoxy resin. 123

Table 4.18 LAC and MAC of the fabricated samples with 0.7 cm and 1.4 cm thickness and 30% weight epoxy resin 125

Table 4.19 LAC and MAC of the fabricated samples with 0.7 cm and 1.4 cm thickness and 25% weight epoxy resin 128

Table 4.20 LAC and MAC of the fabricated samples with 0.7 cm and 1.4 cm thickness and 20% weight epoxy resin. 130

Table 4.21 LAC and MAC of the fabricated samples with 0.7 cm and 1.4 cm thickness and 15% weight epoxy resin. 132

Table 4.22 LAC and MAC of the fabricated samples with 0.7 cm thickness and 10% weight epoxy resin. 134

Table 4.23 Experimental and theoretical mass attenuation coefficients values of lead and the fabricated samples with 15% and 10% epoxy resin and their relative difference. 138

Table 4.24 Linear attenuation coefficient values of the investigated samples with those reported in literature. 141

Table 4.25 Half value layer, tenth value layer, and mean free path of the investigated samples with 0.7 cm and 1.4 cm thickness and 15% epoxy resin. 142

Table 4.26 Half value layer, tenth value layer, and mean free path of the investigated samples with 0.7 cm and 1.4 cm thickness and 10% epoxy resin. 145

Table 4.27 RPE (0.7 cm and 1.4 cm thicknesses, 15% Epoxy resin). 148

Table 4.28 RPE (0.7 cm and 1.4 cm thicknesses, 10% Epoxy resin). 149

Table 4.29 Radiation shielding effectiveness of lead and the fabricated bricks against 140 keV emitted from ^{99m}Tc radioisotope. 152

Table 4.30 Radiation shielding effectiveness of lead and the fabricated bricks against 364 keV emitted from ^{131}I radioisotope. 152

LIST OF FIGURES

Page

Figure 2.1 The ability of different types of radiation to pass through materials (Retrieved from https://opentextbc.ca/chemistry/chapter/21-6-biological-effects-of-radiation/ Data accessed May 2020).....14

Figure 2.2 Electromagnetic spectrum (Retrieved from https://www.cyberphysics.co.uk/topics/light/emspect.htm Data accessed May 2020). 15

Figure 2.3 Gamma ray region of the electromagnetic spectrum (Retrieved from,https://electromagneticspectrumscience.weebly.com/gamma-rays.html Data accessed May 2020). 16

Figure 2.4 Schematic representation of the photoelectric absorption in process. (Retrieved from G. Nelson and D. Reilly, 1991). 18

Figure 2.5 A schematic representation of Compton scattering (Retrieved from G. Nelson and D. Reilly, 1991). 19

Figure 2.6 A schematic representation of pair production (Retrieved from G. Nelson and D. Reilly, 1991).....20

Figure 2.7 Formation of an electron-positron pair. 20

Figure 2.8 Transmission of gamma ray through absorber. 23

Figure 2.9 Linear attenuation coefficient of NaI showing contributions from photoelectric absorption, Compton scattering, and pair production (Retrieved from G. Nelson and D. Reilly, 1991). 24

Figure 2.10 The relative importance of gamma radiation interaction with matter (Retrieved from https://www.radiation-dosimetry.org/what-is-linear-attenuation-coefficient-definition/ Data accessed May 2020).....26

Figure 2.11 Gamma radiation intensity dependence on absorber thickness (Retrieved from https://www.radiation-dosimetry.org/what-is-linear-attenuation-coefficient-definition/ Data accessed May 2020). 26

Figure 2.12 Comparison of gamma shielding materials. (Retrieved from Los Alamos National Laboratory (Martinez *et al*., 2001)). 33

Figure 2.13 Comparison of lightweight gamma shielding material. (Retrieved from Los Alamos National Laboratory (Martinez *et al*., 2001)). 33

Figure 2.14 General manufacturing process for tungsten carbide powder (Retrieved from Fang *et al*., 2014).....39

Figure 3.1 Flow chart of the methodology framework.....48

Figure 3.2 Tungsten carbide-based epoxy mixture placed on the magnetic stirrer. 50

Figure 3.3 A&D weighting GR-200 lab analytical balance. 51

Figure 3.4 Transparent silicone square mould with two defined thicknesses 0.7 cm and 1.4 cm. 51

Figure 3.5 Transparent silicone rectangular mould. 55

Figure 3.6 Schematic diagram of FESEM. Retrieved from (Billah, 2016). 57

Figure 3.7 Extreme High Resolution Field Emission Scanning Electron Microscope (XHR-FESEM) Model FEI Verios 460L. 58

Figure 3.8 Gatan Precision etching coating system Model 682. 58

Figure 3.9 Schematic diagram of EDX spectroscopy. Retrieved from (Islam *et al*., 2018). 60

Figure 3.10 Tungsten carbide epoxy composites samples for FESEM/EDX analysis test. 61

Figure 3.11 Tungsten carbide cobalt epoxy composites samples for FESEM/EDX analysis test. 61

Figure 3.12 Tungsten carbide/barium sulphate/epoxy composites samples for FESEM/EDX analysis test. 62

Figure 3.13 Tungsten carbide/bismuth oxide/epoxy composites samples for FESEM/EDX analysis test. 63

Figure 3.14 Schematic diagram of FTIR spectroscopy. Retrieved from (Jalvandi, 2016). 64

Figure 3.15 400 Spotlight Fourier transform infrared spectroscopy. 65

Figure 3.16 Spectrum of the mid IR region. Retrieved from (Hynes *et al*., 2005). 66

Figure 3.17 Block diagram of gamma spectroscopy system with NaI detector. Retrieved from (Akkurt *et al*., 2014). 68

Figure 3.18 Illustration of NaI (TI) detector and Photomultiplier tube. Retrieved from (https://scionix.nl/read-out/). 69

Figure 3.19 The radiation sources used in gamma spectroscopy experiment with their corresponding activities. 71

Figure 3.20 The experimental setup for the attenuation measurements. 71

Figure 3.21 The experimental setup for the attenuation measurements with sample placed between radiation source and detector. 72

Figure 3.22 Schematic illustration of Gamma camera. Retrieved from (Ozdemir *et al*., 2019). 73

Figure 3.23 Discovery NM/CT670 SPECT. 74

Figure 3.24 Dose calibrator (BIODEX—ATOMLAB 500). 75

Figure 3.25 The experimental setup of the SPECT scanning technique for evaluation of the fabricated bricks. 76

Figure 3.26 Schematic diagram of Vickers hardness test. Retrieved from http://www.substech.com/dokuwiki/doku.php?id=hardness_test_methods#vickers_hardness_test Data accessed October 2021). 78

Figure 3.27 Vickers hardness test process. (Retrieved from https://www.tec-science.com/material-science/material-testing/vickers-hardness-test/ Data accessed October 2021). 78

Figure 3.28 Microhardness Tester (Model: LM248AT). 79

Figure 3.29 Sample under hardness testing. 82

Figure 4.1 Tungsten carbide-based epoxy composites (Top: 1.4 cm thickness. Bottom: 0.7 cm thickness)..... 85

Figure 4.2 Tungsten carbide cobalt-based epoxy composites (Top: 1.4 cm thickness. Bottom: 0.7 cm thickness)..... 85

Figure 4.3 Tungsten carbide barium sulphate-based epoxy resin composites (Top: 1.4 cm thickness. Bottom: 0.7 cm thickness). 85

Figure 4.4 Tungsten carbide bismuth oxide-based epoxy resin composites (Top: 1.4 cm thickness. Bottom: 0.7 cm thickness). 86

Figure 4.5 Tungsten carbide cobalt-based epoxy (A, B, C, and D) and tungsten carbide-based epoxy bricks (E, F, G, and H) (Top: 1.4 cm thickness. Bottom: 0.7 cm thickness). 87

Figure 4.6 Tungsten carbide cobalt-based epoxy (A, B, C, and D) and tungsten carbide-based epoxy bricks (E, F, G, and H) (Top: 1.4 cm thickness. Bottom: 0.7 cm thickness). 87

Figure 4.7 Tungsten carbide barium sulphate-based epoxy resin bricks (I, J) (Top: 1.4 cm thickness. Bottom: 0.7 cm thickness), WC-$BaSO_4$-E7 right, WC-$BaSO_4$-E6 left (K, L). 88

Figure 4.8 Tungsten carbide barium sulphate-based epoxy resin bricks (I, J) (Top: 1.4 cm thickness. Bottom: 0.7 cm thickness), WC-$BaSO_4$-E7 right, WC-$BaSO_4$-E6 left (K,L). 88

Figure 4.9 Tungsten carbide/Bismuth oxide/Epoxy resin bricks (M, N) (Top: 1.4 cm thickness. Bottom: 0.7 cm thickness), WC-Bi_2O_3-E7 right, WC-Bi_2O_3-E6 left (O, P). 89

Figure 4.10 Tungsten carbide Bismuth oxide-based Epoxy resin bricks (M, N) (Top: 1.4 cm thickness. Bottom: 0.7 cm thickness), WC-Bi_2O_3-E7 right, WC-Bi_2O_3-E6 left (O, P). 89

Figure 4.11 Variation of the measured densities values of the fabricated samples with respect to filler loading..... 91

Figure 4.12 Density values of all fabricated samples. 92

Figure 4.13 Variation of effective atomic number values for the investigated samples as a function of energy at 0.7 cm thicknesses. 98

Figure 4.14 Variation of effective atomic number values for the investigated samples as a function of energy at 1.4 cm thicknesses. 98

Figure 4.15 FESEM image of epoxy resin. 10000X magnification (a), 80000X magnification (b). 100

Figure 4.16 FESEM image of Tungsten carbide powder. 2500X magnification (a), 10000X magnification (b), 40000X magnification (c), 53333X magnification (d). 101

Figure 4.17 FESEM image of Tungsten carbide cobalt powder. 10000X magnification (a), 25000X magnification (b), 100000X magnification (c), 200000X magnification (d). 102

Figure 4.18 FESEM image of Barium sulphate powder. 25000X magnification (a), 10000X magnification (b), 40000X magnification (c), 80000X magnification (d). 103

Figure 4.19 FESEM image of Bismuth oxide powder. 2500X magnification (a), 10000X magnification (b), 40000X magnification (c), 80000X magnification (d). 104

Figure 4.20 FESEM images of the fractures surface of tungsten carbide epoxy resin composites, with 35% epoxy resin weight percentage at 5 mm resolution (a), 25% epoxy resin weight percentage at 5 micrometre resolution (b), 15% epoxy resin weight percentage at 500 nm resolution (C), and 10% epoxy resin weight percentage at 5 mm resolution. 105

Figure 4.21 FESEM images of the fractures surface of tungsten carbide cobalt epoxy resin composites, with 35% epoxy resin weight percentage at 1 micro (a), 25% epoxy resin weight percentage at 500 nano (b), 15% epoxy resin weight percentage at 5 micrometer (C), and 10% epoxy resin weight percentage at 5 micro meter. 106

Figure 4.22 FESEM images of the fractures surface of tungsten carbide/barium sulphate/epoxy resin composites, with 10% epoxy

resin weight percentage at 5 micro (a), 15% epoxy resin weight percentage at 5 micro (b), 25% epoxy resin weight percentage at 5 micrometer (C), and 35% epoxy resin weight percentage at 5 micro meter. 107

Figure 4.23 FESEM images of the fractures surface of tungsten carbide/bismuth oxide/epoxy resin composites, with 10% epoxy resin weight percentage at 5 micro (a), 15% epoxy resin weight percentage at 5 micro (b), 25% epoxy resin weight percentage at 5 micrometer (C), and 35% epoxy resin weight percentage at 5 micro meter. 108

Figure 4.24 Vickers hardness values of the investigated samples with 0.7 cm thickness. 110

Figure 4.25 Vickers hardness value of the investigated samples with 1.4 cm thickness. 110

Figure 4.26 FTIR spectrum of epoxy resin sample. 112

Figure 4.27 FTIR spectrum of tungsten carbide epoxy resin composite (WCE). 113

Figure 4.28 FTIR spectrum of tungsten carbide cobalt epoxy resin composite (WC-CoE). 113

Figure 4.29 FTIR spectrum of tungsten carbide barium sulphate epoxy resin composite (WC-$BaSO_4$E).....114

Figure 4.30 FTIR spectrum of tungsten carbide bismuth oxide epoxy resin composite (WC-Bi_2O_3E). 114

Figure 4.31 Energy calibration test for photon energy versus window number. 117

Figure 4.32 ^{241}Am spectrum obtained using NaI (TI) detector with (SCA) single channel analyser. 118

Figure 4.33 ^{133}Ba spectrum obtained using NaI (TI) detector with (SCA) single channel analyser. 118

Figure 4.34 ^{22}Na spectrum obtained using NaI (TI) detector with (SCA) single channel analyser. 119

Figure 4.35 ^{137}Cs spectrum obtained using NaI (TI) detector with (SCA) single channel analyser. 119

Figure 4.36 ^{60}Co spectrum obtained using NaI (TI) detector with (SCA) single channel analyser. 120

Figure 4.37 Mass attenuation coefficients of the investigated samples with 40% epoxy resin and 0.7 cm thickness with respect to gamma photon energy.....122

Figure 4.38 Mass attenuation coefficients of the investigated samples with 40% epoxy resin and 1.4 cm thickness with respect to gamma photon energy.....122

Figure 4.39 Mass attenuation coefficients of the investigated samples with 35% epoxy resin and 0.7 cm thickness with respect to gamma photon energy.....124

Figure 4.40 Mass attenuation coefficients of the investigated samples with 35% epoxy resin and 1.4 cm thickness with respect to gamma photon energy.....124

Figure 4.41 Mass attenuation coefficients of the investigated samples with 30% epoxy resin and 0.7 cm thickness with respect to gamma photon energy.....126

Figure 4.42 Mass attenuation coefficients of the investigated samples with 30% epoxy resin and 1.4 cm thickness with respect to gamma photon energy.....127

Figure 4.43 Mass attenuation coefficients of the investigated samples with 25% epoxy resin and 0.7 cm thickness with respect to gamma photon energy.....129

Figure 4.44 Mass attenuation coefficients of the investigated samples with 25% epoxy resin and 1.4 cm thickness with respect to gamma photon energy.....129

Figure 4.45 Mass attenuation coefficients of the investigated samples with 20% epoxy resin and 0.7 cm thickness with respect to gamma photon energy.....131

Figure 4.46 Mass attenuation coefficients of the investigated samples with 20% epoxy resin and 1.4 cm thickness with respect to gamma photon energy. 131

Figure 4.47 Mass attenuation coefficients of the investigated samples with 15% epoxy resin and 0.7 cm thickness with respect to gamma photon energy. 133

Figure 4.48 Mass attenuation coefficients of the investigated samples with 15% epoxy resin and 1.4 cm thickness with respect to gamma photon energy. 134

Figure 4.49 Mass attenuation coefficients of the investigated samples with 10% epoxy resin and 0.7 cm thickness with respect to gamma photon energy. 135

Figure 4.50 Mass attenuation coefficients of the investigated samples with 10% epoxy resin and 1.4 cm thickness with respect to gamma photon energy. 136

Figure 4.51 Theoretical and experimental mass attenuation coefficient values of the investigated samples of 15% epoxy with respect to energy. . 139

Figure 4.52 Theoretical and experimental mass attenuation coefficient values of the investigated samples of 15% epoxy with respect to energy. . 139

Figure 4.53 Variation of half value layer values for the investigated samples as a function of energy at 1.4 cm thicknesses. 143

Figure 4.54 Variation of tenth value layer values for the investigated samples as a function of energy at 1.4 cm thicknesses. 143

Figure 4.55 Variation of mean free path values for the investigated samples as a function of energy at 1.4cm thicknesses. 144

Figure 4.56 Variation of half value layer values for the investigated samples as a function of energy at 1.4 cm thicknesses. 146

Figure 4.57 Variation of tenth value layer values for the investigated samples as a function of energy at 1.4 cm thicknesses. 146

Figure 4.58 Variation of mean free path values for the investigated samples as a function of energy at 1.4 cm thicknesses. 147

Figure 4.59 Variation of radiation shielding efficiency values for the investigated samples as function of energy at 0.7 cm and 1.4 cm thicknesses. 149

Figure 4.60 Variation of radiation shielding efficiency values for the investigated samples as function of energy at 0.7 cm and 1.4 cm thicknesses. 150

Figure 4.61 Comparison of radiation shielding effectiveness between lead and the fabricated bricks against 140 keV emitted from ^{99m}Tc radioisotope. 153

Figure 4.62 Comparison of radiation shielding effectiveness between lead and the fabricated bricks against 364 keV emitted from ^{131}I radioisotope. 154

Figure 4.63 Comparison of radiation shielding effectiveness between different thicknesses of lead and the fabricated bricks against 364 keV emitted from ^{131}I radioisotope. 155

LIST OF SYMBOLS

^{241}Am	Isotope of americium
^{133}Ba	Isotope of barium
^{137}Cs	Radioactive isotope of cesium
^{60}Co	Radioactive isotope of cobalt
^{131}I	Radioisotope of iodine
^{22}Na	Sodium manmade isotope
^{99m}Tc	Metastable nuclear isomer of technetium-99
C	Carbon
Cl	Chlorine
cm^{-1}	A reciprocal centimeter
Cps	Centipoise
eV	Electronvolt
Hz^{-1}	Hertz
keV	Kiloelectron volts
Kgf/mm^2	Kilogram-force/square millimetre
kV	Kilovoltage
MBq	Mega becquerel
MeV	Megaelectron volt
O	Oxygen
^{o}C	Degree Celsius
Pb	Lead
S	Sulphur
Z	Atomic number
Z_{eff}	Effective atomic number

B	Beta
γ	Gamma
λ	Relaxation time
μ	Linear attenuation coefficients
μ/ρ	Mass attenuation coefficient
ρ	Density

LIST OF ABBREVIATIONS

AMDI	Advanced Medical and Dental Institute
ANOVA	Analysis of Variance
APS	Aerodynamic Particle Sizer
ARC	Animal Research Complex
ASTM	American Society for Testing and Materials
$BaSO_4$	Barium Sulphate
Bi_2O_3	Bismuth Oxide
CTC	Clinical Trial Complex
EDX	Energy Dispersive X-Ray Spectroscopy
FESEM	Field Emission Scanning Electron Microscopy
FTIR	Fourier Transform Infrared Spectroscopy
HEGP	High Energy General Purpose
HVL	Half Value Layer
LAC	Linear Attenuation Coefficient
LEHR	Low Energy High Resolution
MAC	Mass Attenuation Coefficient
MCA	Multichannel Analyser
MCB	Miniature Circuit Breaker
MFP	Mean Free Path
NaI (TI)	Thallium Activated Sodium Iodide
NIST	National Institute of Standards and Technology
PMT	Photomultiplier Tube
RoHS	Restriction of Hazardous Substances Directive
RPE	Radiation Protection Efficiency

SCA	Single Channel Analyser
SEM	Scanning Electron Microscopy
SPECT	Single Photon Emission Computed Tomography
TVL	Tenth Value Layer
UKM	Universiti Kebangsaan Malaysia
USM	Universiti Sains Malaysia
WC	Tungsten Carbide
WC-$BaSO_4$-E	Tungsten Carbide Barium Sulphate-Based Epoxy Resin
WC-Bi_2O_3-E	Tungsten Carbide Bismuth Oxide-Based Epoxy Resin
WC-Co	Tungsten Carbide Cobalt
WC-CoE	Tungsten Carbide Cobalt-Based Epoxy Resin
WCE	Tungsten Carbide-Based Epoxy Resin
XCOM	Photon Cross Sections Data Base

LIST OF APPENDICES

Appendix A EDX spectrum of the proposed materials and composites.

Appendix B Energy calibration of the spectrometer.

Appendix C Attenuation coefficients of the fabricated composites.

Appendix D Raw data of statistical analysis.

PEMBANGUNAN BATA POLIMER BERASASKAN TUNGSTEN KARBIDA BEBAS PLUMBUM SEBAGAI PERISAI SINAR GAMA

ABSTRAK

Batu bata plumbum ialah bentuk perisai sinar gamma yang paling banyak digunakan di jabatan radiologi diagnostik, radioterapi dan perubatan nuklear. Walau bagaimanapun, plumbum adalah berat, toksik, dan berbahaya kepada kesihatan manusia. Perisai sinaran berasaskan polimer boleh digunakan dalam bidang perisai sinaran kerana sifat fizikal dan kimianya yang sangat baik, mudah untuk difabrikasi, kos pembuatan yang rendah dan kukuh. Selain itu, sifat pelindung sinaran mereka boleh dipertingkatkan dengan menggunakan pengisi yang mempunyai nombor atom yang tinggi. Tujuan penyelidikan ini adalah untuk membangunkan bata polimer berasaskan tungsten karbida bebas plumbum sebagai perisai sinaran gamma. Pembuatan komposit polimer berasaskan tungsten karbida melibatkan pencampuran serbuk tungsten karbida dan serbuk kobalt tungsten karbida dengan resin epoksi pada peratusan berat yang berbeza (60, 65, 70, 75, 80, 85, 90) yang berperanan sebagai pengisi. Selain itu juga, penambahan bismut oksida dan serbuk barium sulfat kepada matriks epoksi berasaskan tungsten karbida telah dikaji. Sifat-sifat fizikal, morfologi, kimia, mekanikal dan perlindungan foton telah disiasat untuk semua komposit yang direka. Kombinasi serbuk epoksi yang paling optimum antara semua sampel ialah dengan 85 dan 90 peratusan berat pengisi. Analisis mikrostruktur menunjukkan bahawa pengisi diagihkan secara seragam dalam matriks epoksi. Beberapa aglomerasi telah diperhatikan untuk komposit yang mempunyai lebih daripada 75% berat pengisi. Spektroskopi inframerah transformasi Fourier digunakan untuk mengkaji sifat kimia komposit yang direka. Spektrum penyerapan FTIR bagi setiap

sampel dianalisis dalam julat 600-4000 cm^{-1}. Keputusan yang diperolehi tidak menunjukkan sebarang perubahan spektrum bagi semua sampel. Sifat mekanikal komposit epoksi meningkat pada mulanya dengan peningkatan dalam beban pengisi, kecuali komposit epoksi berasaskan kobalt tungsten karbida, kekerasan menunjukkan penurunan dengan peningkatan beban pengisi. Nilai kekerasan Vickers WC-CoE pada ketebalan 0.7 cm masing-masing adalah 36.74 dan 40.30 kgf/mm^2 untuk resin epoksi 10% dan 15%, manakala nilai kekerasan Vickers bagi ketebalan 1.4 cm ialah 33.83 kgf/mm^2 dan 37.86 kgf/mm^2 masing-masing adalah 2 % dan 15% resin epoksi. Pemerhatian daripada spektroskopi gamma menunjukkan keputusan bahawa kecekapan pelindung sinaran bagi komposit epoksi berasaskan tungsten karbida bertambah baik dengan penambahan serbuk bismut oksida. Sebaliknya, tidak terdapat perbezaan yang signifikan dengan penambahan sebatian barium sulfat ke dalam matriks kerana barium sulfat mempunyai ketumpatan paling sedikit antara semua pengisi serbuk yang digunakan dalam kajian ini. Keberkesanan perisai sinaran bagi bata rekaan telah dinilai menggunakan SPECT pada 140 keV dan 364 keV. Keputusan daripada eksperimen pengesahan bata rekaan menunjukkan bahawa bata resin epoksi berasaskan tungsten karbida boleh menggantikan plumbum pada julat sinar gamma tenaga rendah sehingga 140 keV, manakala bata polimer yang lebih tebal diperlukan untuk perlindungan daripada tenaga sinar gamma yang lebih tinggi.

DEVELOPMENT OF LEAD-FREE TUNGSTEN CARBIDE-BASED POLYMERIC BRICKS AS GAMMA RADIATION SHIELDING

ABSTRACT

Lead bricks are the most widely used form of gamma ray shields in diagnostic radiology, radiotherapy, and nuclear medicine departments. However, lead is heavy, toxic, and dangerous to human health. Polymer-based radiation shields can be utilised in radiation shielding field due to their excellent physical and chemical properties, ease of fabrication, low manufacturing costs, and toughness. Also, their radiation shielding properties can be improved by using high atomic number fillers. The purpose of this research was to develop a lead-free tungsten carbide-based polymeric bricks as gamma radiation shielding. The fabrication of tungsten carbide-based polymeric composites involved mixing tungsten carbide powder and tungsten carbide cobalt powder with epoxy resin at different weight percentages (60, 65, 70, 75, 80, 85, 90) of fillers. Also, addition of bismuth oxide and barium sulphate powder to tungsten carbide-based epoxy matrix were studied. The physical, morphological, chemical, mechanical, and photon shielding properties were investigated for all the fabricated composites. The most optimum powder epoxy combination among all samples were 85 and 90 weight percentage of fillers. The microstructural analysis indicated that the fillers distributed uniformly within the epoxy matrix. Some agglomerations were observed for composites having more than 75 wt% of filler. Fourier transform infrared spectroscopy was used to study the chemical properties of the fabricated composites. FTIR absorption spectrum of each sample analysed in the range of 600-4000 cm^{-1}. The results obtained did not show any spectral change for all samples. The mechanical properties of epoxy composites

increased initially with an increase in the filler loading, except the tungsten carbide cobalt-based epoxy composites, the hardness showed a decrease with increasing filler loading. The Vickers hardness values of WC-CoE at 0.7 cm thickness were 36.74 and 40.30 kgf/mm^2 for 10% and 15% epoxy resin respectively, while the Vickers hardness values at 1.4 cm thickness were 33.83 kgf/mm^2 and 37.86 kgf/mm^2 for 10% and 15% epoxy resin respectively. It was observed from gamma spectroscopy results that the radiation shielding efficiency of tungsten carbide-based epoxy composites improved with the addition of bismuth oxide powder. On the other hand, there was no significant difference observed with the addition of barium sulphate compound to the matrix as barium sulphate has the least density among all powder fillers used in this study. Radiation shielding effectiveness of the fabricated bricks were evaluated using SPECT at 140 keV and 364 keV. Results from the validation experiment of the fabricated bricks indicated that tungsten carbide-based epoxy resin bricks can replace lead at low energy gamma ray range up to 140 keV, while thicker polymeric bricks required for shielding against higher gamma ray energies.

CHAPTER 1

INTRODUCTION

1.1 Background

The word radiation used to describe the electromagnetic waves until the beginning of the twentieth century (Bushberg *et al*., 2012). Since then, the term radiation has come to apply to the entire electromagnetic spectrum, which includes all known atomic and subatomic particles (Tsoulfanidis *et al*., 2015). The higher frequencies of the electromagnetic spectrum consists of x-rays and gamma rays which are types of ionising radiation while lower frequencies such as ultraviolet, infrared, microwave, and radiofrequency are types of non-ionising radiation. The difference between these two types of radiation is determined by their energy level. Non-ionisation refers to energy that is sufficient enough to excite atoms or electrons but insufficient to remove electrons from their orbitals. The ultraviolet region is the highest energy range among the non-ionising category (McColl *et al*., 2015). Non-ionising radiation can be found in a wide range of occupational settings including power grid and power transmission networks, television and radio transmitters, cellular radio base stations, microwave ovens, computer monitors, wireless routers, batteries, and cell phones (Ziegelberger *et al*., 2020).

High-energy radiation such as gamma rays and neutron radiation can be found in many sectors including healthcare, aviation industries, and nuclear power plants (Donya *et al*., 2015). Ionising radiation interacts with matter by transferring energy from the electron or molecule to the atom through collisions with target atoms. Depending on the energy of the incident photon and the density of the target material, the energy transfer can result in excitation, ionisation, and heat generation. In other words, radiation interaction with matter, particularly biological matter, can

lead to long-lasting, permanent health consequences (The National Academies of Sciences, 2005). Radioactive sources that emit gamma radiation are widely used in nuclear medicine departments, as a result, radiation shielding garments and bricks that made of lead are commonly used to protect against gamma rays at these facilities. However, lead is considered as heavy metal, and it is known for its toxicity that may have serious harmful effects on health and environment. As a result, development of radiation shielding technology is considered indispensable field, especially the development of lead-free and environmentally friendly materials with various composites. The selection of shielding material is based on several factors, including the weight and thickness of the material, the shielding performance, the availability of the material, the uniformity capacity, the heat dissipation, and the resistance to radiation damage.

For a variety of reasons, lead was regarded as the optimum material for radiation shielding in the past. Lead is particularly effective in shielding against radiation sources, making it a standard in the construction of radiation protection systems. Lead has high density, and standard radiation shields made of lead has been used for centuries as a conventional shielding material for high energy radiation shielding (Asal *et al.*, 2021). Unfortunately, there are many drawbacks of using lead, the most serious of which being its toxicity to human and environment. Due to the long-term health issues associated with the use of lead or lead compounds as shielding materials, their usage as shielding materials has become increasingly sensitive (Huo *et al.*, 2021). According to the European Union's RoHS (Restriction of Hazardous Substances) directive, the use of lead in various types of equipment and applications has been restricted because of its toxicity (Union *et al.*, 2019) (European Parliament, 2011). As a result, substantial research has been devoted to

the development of novel shielding materials that are safer and easier to handle (Belgin *et al.*, 2015).

Radiation protection considered as one of the most important elements associated with radiation environment. The type of radiation to be blocked or attenuated determines the composition of the material used for radiation safety. The processes by which various forms of radiation interact with matter are well documented and they serve as the foundation for choosing the right shielding material.

Gamma rays in the diagnostic range up to hundreds of keV can be effectively attenuated by shielding them with a high atomic number material of appropriate thickness (K. S. Mann, 2017). This is because the gamma photons lose energy as they interact with heavy atoms (Khan, 2014). Lead and lead-based alloys are frequently used as radiation shielding materials. Lead, on the other hand, is toxic and can cause serious health problems if used for an extended period. Moreover, it is heavy as well, posing occupational health risks such as back pain, improper posture, and so forth (Burns *et al*., 2017; Hyun *et al*., 2016; Finnerty & Brennan, 2005).

Ideal radiation shielding should be lead-free and lead equivalent as well (Jones *et al.*, 2015) because lead served as a reference point for comparing the attenuation properties of the shielding material to those of pure lead of a specified thickness (McCaffrey *et al*., 2007). In this study, tungsten carbide-based epoxy resin composites were fabricated and compared to lead especially in their ability to attenuate gamma radiation. Four different composites were investigated including tungsten carbide-based epoxy resin composite, tungsten carbide cobalt-based epoxy

resin composite, tungsten carbide barium sulphate-based epoxy resin composite, and tungsten carbide bismuth oxide-based oxy resin composite.

Polymer composites can be effectively developed in such a way that provides efficient, lead-free yet lead-equivalent gamma ray shielding (Tiwari *et al*., 2009; Zhang *et al*., 2004; O'Rourke *et al*., 2002). It has been reported that polymers reinforced with micro, and nanoparticles exhibit enhanced material properties, including improved mechanical strength and thermal properties, as well as improved radiation resistance (Tiwari *et al*., 2012; Tiwari *et al*., 2009; Zhang & Fang, 2005). The material used for radiation shielding is determined by the type of radiation source. The production of novel materials for radiation shielding is in high demand in the field of nuclear medicine (Lim-aroon *et al.*, 2019). The use of harmful heavy metals such as lead has long-term negative effects on human health and the environment. As a result, it boosts interest in developing non-toxic, lightweight, durable, and economically viable radiation shielding products to replace lead. There is an immediate need to substitute lead radiation shielding material for radiation protection (Abualroos *et al*., 2019; Rudolph *et al*., 2011). Lead-free compounds such as tungsten are non-toxic (Rieck, 2013). Additionally, owing to its greater atomic number, tungsten has a higher density and superior shielding properties than lead (Luković *et al*., 2015). However, pure tungsten is very costly. In comparison to conventional lead shielding material, pure tungsten has higher attenuation properties and a smaller half value layer (Division, 2014).

In the past few years, researchers studied shielding efficiency of tungsten and tungsten compounds. A study on ultra-high molecular weight polyethylene with the inclusion of tungsten powder revealed that UHMWP is one of the most robust

polymers to ionising radiation (Selyutin *et al*., 2010). The incorporation of tungsten particles into the ultrahigh molecular weight polyethylene structure improved its shielding properties. The attenuation coefficient increases as the tungsten content of the composite increases (Kaloshkin *et al*., 2012). For low intensity gamma rays, the radiation shielding properties of tungsten and epoxy composites were studied (Chang *et al*., 2015). The results indicated that a high tungsten content improves the sample's radiation shielding properties. Due to its non-toxic qualities, this research demonstrated that tungsten is a potential material to replace conventional lead, and it is highly efficient at attenuating neutron radiation as well (Islam *et al*., 2017; Singh *et al*., 2015; Lukovi *et al*., 2014).

Efficacy of tungsten carbide as lead free radiation shielding material in nuclear medicine has been evaluated by analysing its attenuation properties (Abualroos *et al*., 2020). Additionally, Soylu *et al*. demonstrated that the radiation shielding performance of a tungsten carbide and ethylene vinyl acetate polymer composite was comparable to that of lead at 364 keV and 662 keV gamma photon energies (Soylu *et al*., 2015). As a result, there is an imminent need to substitute the conventional lead radiation shielding material with safe, lead-free and environmentally friendly composites that have same attenuation efficiency of lead.

This research work focuses on the evaluation of the efficacy of tungsten carbide and other additives mixed with epoxy resin as new lead-free radiation shielding material in nuclear medicine. Those additives including bismuth oxide and barium sulphate. Bismuth oxides are quite interesting for any application that requires a high level of radiopacity as well as a high level of biocompatibility (Shahbazi *et al*., 2020). They have been widely used for a variety of purposes,

including cosmetic, industrial, laboratory, and pharmaceutical (Yang *et al*., 2018; Wang *et al*., 2018; Wang *et al*., 2017). Bismuth is a widely known nontoxic alternative to lead in brass plumbing fixtures, fishing sinkers, free-machining steels, and solders, as well as a foundry metallurgical additive (Li *et al*., 2012). Significant applications of bismuth in medicine and health care are related to its high efficacy in treating burns, intestinal disorders, and stomach ulcers, as well as its potential activity against microorganisms, viruses, and malignant tumours (Chan *et al*., 2019; Li *et al*., 2019; Hong *et al*., 2015).

Barium sulphate has been used in orthopedic medicine, diagnostic imaging and other applications. It has been used as a contrast media to allow enhanced visualisation of tissue and normal or defect organs by increasing the absorption of x-rays as they passed throughout the body (Aninwene *et al*., 2013). The toxicity of barium is related to the salt's solubility and thus availability. Because barium sulphate is insoluble, it is considered non-toxic (Konduru *et al*., 2014).

1.2 Problem statement

Efficient use of nuclear radiation can be achieved by avoiding the unnecessary radiation exposure, which in turns requires development of radiation shielding materials. Lead considered as the primary radiation shielding material due to its physical and mechanical properties. However, there are several drawbacks along the past years while providing radiation protection.

The use of lead as shielding material poses a serious safety and health issues in the field of radiation protection. The radioactive tracers used in nuclear medicine generate gamma radiation. This gamma radiation has a high penetrating power. Lead is commonly utilised as a radiation shielding material in nuclear medicine because of

its high ability to protect against gamma rays (Cunningham, 2007). The accumulation of dust on the surface of lead objects, however, can make this radiation shielding material harmful. Lead dust can become airborne and be inhaled or swallowed by human accidently (Ali *et al*., 2012).

Furthermore, lead dust on workers' skin and clothing may be brought home from work, which is referred to as take-home exposure; it settles on surfaces and is inhaled or ingested by young children with normal mouthing behaviours (Burns *et al*., 2016). A study done by Hulbert *et al*., showed that lead dust is a major source of lead exposure, it can be taken in through the lungs and gastrointestinal tract (Hulbert *et al*., 2009). Lead enters the bloodstream following absorption, where it transforms into a potent and diverse poison.

In addition, lead has been shown to have an effect on the central and peripheral neurological systems, bone marrow, kidneys, myocardium, endocrine, and immunological systems. Moreover, lead dust can contaminate floors and other adjacent work surfaces (Dehghan *et al*., 2014; Taylor *et al*., 2012). In nuclear medicine department, lead bricks used as radiation shielding, when handling or working with lead bricks, the most common way in which lead enters the body is via inhalation of airborne lead particles (Materna *et al*., 2004). When a lead brick is moved, lead dust is created, and it can be inhaled into the lungs and upper respiratory tract (Stevenson *et al*., 2008; Papanikolaou *et al*., 2005; Martinez *et al*., 2001). Lead is neither biodegradable nor quickly excreted from the body, making its effects long term and cumulative. Human exposure to lead can induce toxic effects on hematological, cardiovascular, nervous and reproductive systems.

The adverse health effects of lead exposure in children and adults are also well documented (Healey *et al*., 2009; Oteiza, 2008; Vaziri, 2008; Navasacien *et al*., 2007; Heath *et al*., 2003). Workers are protected from radiation by wearing lead-equivalent shields, often known as lead aprons. The lead sheets and covering layers might crack and lose their effectiveness as a shield against dispersed ionising radiation as a result of daily use, bending, or inappropriate handling (Smith *et al*., 2016) For these reasons, shields are frequently tested for gaps and cracks and those found to be unsuitable are withdrawn from circulation (Humphry *et al*., 2018).

In addition, several types of cumulative trauma disorder are possible in the clinical setting in nuclear medicine because of the heavy weight of lead bricks used in the clinical setting. For example, Myalgia is pain in one or more muscles, and tendonitis is inflammation of a tendon. Epicondylitis involves inflammation of and pain in certain bony prominences in the area of the elbow, usually resulting from excessive strain on and twisting of the forearm (Bolus, 2019). It is well-established that exposure to lead can promote the development of several diseases and disorders through different mechanisms of toxicity (Fenga *et al*., 2017; Hengstler *et al*., 2003). The hypothesis that the immune system represents a critical target for lead-induced toxicity has been suggested by epidemiological and experimental studies (Fenga *et al*., 2017; Park *et al*., 2008; Martinez & Cournoyer, 2001). The reproductive system of both males and females is affected by chronic, high-dose exposures of lead (Wani *et al*., 2015). Toxic levels of lead can lead to miscarriages, prematurity, low birth weight, and problems with development during childhood (Cleveland *et al*., 2008; Asic *et al*., 2008).

Concrete was used as radiation shielding material too. However, its expensive cost, the composition's inconsistency, and its capacity to crack due to heat absorption give concern to look for alternative shielding materials (Mahesh *et al*., 2015). In the era of finding the suitable shielding material, unavailability, health hazards, and cost are the main constraints to be considered. To overcome all these drawbacks, an available, cost-effective, and environmentally friendly shielding materials should be evaluated. Moreover, material with high density and atomic number that can be used at large energy scaled is preferred for radiation shielding.

Recently, researchers tended to investigate radiation shielding capacity of various new radiation shielding materials. Thus, this study focused on testing shielding features of polymer-based compounds in order to design and fabricate excellent shielding materials. In nuclear medicine, there is a high demand for the development of novel materials for radiation shielding. Polymer composites can be thought of as a viable solution. Radiation shielding applications, on the other hand, necessitate the careful selection of both the appropriate polymer matrix and the filler material to develop efficient radiation shielding materials. In this study, tungsten carbide powder, tungsten carbide cobalt powder, barium sulphate, and bismuth oxide of different percentages mixed with epoxy resin polymer to evaluate the ability of the resultant polymer mixture in shielding gamma ray.

1.3 Research objectives

The main objective of this study was to develop a novel, light weighted, and more effective radiation shielding lead-free tungsten carbide-based polymeric bricks that protect workers and patients against gamma radiation in nuclear medicine unit.

The specific objectives of this study were to:

i. fabricate tungsten carbide-based epoxy resin bricks from the optimum combination percentage of powder and epoxy resin in the matrix based on gamma spectroscopy results
ii. characterise the physical, morphological, and mechanical properties of the fabricated tungsten carbide-based epoxy resin composites.
iii. evaluates the structural properties of epoxy and powders by using Fourier transform infrared spectroscopy.
iv. measures the radiation shielding effectiveness of the fabricated composites by gamma spectroscopy system at different thicknesses and energy range.
v. evaluate the performance of the final fabricated bricks in comparison to conventional lead brick at 140 keV and 364 keV using Single Photon Emission Computed Tomography (SPECT).

1.4 Scope of the study

In nuclear medicine, shielding is necessary when working with a radionuclide that emits gamma rays. In this study, the performance ability of polymer composites to shield against gamma radiation in nuclear medicine was evaluated.

Tungsten carbide powder, tungsten carbide-cobalt powder, barium sulphate powder, bismuth oxide powder, and epoxy resin polymer were evaluated for their physical, chemical, and morphological properties. The physical and morphological properties of the proposed materials evaluated by field emission scanning electron microscopy with energy dispersive x-ray spectroscopy (FESEM/EDX). Homogeneity of the filler distribution in epoxy resin matrix was also investigated by FESEM.

Molecular structure properties and chemical bonds of the samples were investigated by using Fourier transform infrared spectroscopy (FTIR). The hardness characteristic of the fabricated composites was evaluated by microhardness tester. The measurements of radiation shielding properties were performed by using gamma spectroscopy system. Validation of the final fabricated bricks shielding performance was evaluated and compared with conventional lead.

1.5 Structure of the study

This thesis comprises of five chapters. Chapter 1 introduces shielding protection, shielding materials and a brief history of polymers as radiation shielding materials. The problem statement, research objectives and scope of research are also explained in chapter one. It gives a brief explanation about the research topic and the rational of the study.

Chapter 2 presents a comprehensive review of theoretical background and concise literature review of theories, formulas and concepts that are relevant and being used in the subject area of this study. It also provides a literature from previous work that focuses on polymers as gamma radiation shielding.

Chapter 3 describes a detailed materials and methodology involved in radiation shielding bricks fabrication. The effect of adding $BaSO_4$ and Bi_2O_3 to tungsten carbide epoxy resin composite to enhance its properties. This chapter covers all the equipment used in this study as well including magnetic stirrer, FESEM/EDX, gamma spectrometry system, Fourier transform infrared spectroscopy, microhardness tester, and SPECT. The fabrication process and the evaluation performance of the fabricated bricks are explained in detail.

Chapter 4 explains the results and discussion of all the experiments performed in this study. It focuses on results obtained from experimental and samples characterisation. The density, effective atomic numbers, linear and mass attenuation coefficients, half value layer, tenth value layer, mean free path, radiation protection efficiency, chemical properties and mechanical properties sections of all samples were also discussed. Moreover, it also covers detailed discussion on the validation performance of the new developed radiation shielding bricks.

Finally, Chapter 5 presents summary of the study, limitation of the work and further recommendations for future work.

CHAPTER 2

LITERATURE REVIEW

2.1 Introduction

This chapter comprises a detailed review of available research work on ionising radiation and radiation shielding, as well as concepts and theories related to this study. In addition, the conventional radiation shielding, polymer-based composites radiation shielding materials, and the characterisation equipment used to characterise the radiation shielding materials were briefly reviewed.

2.2 Ionising radiation

Photons and subatomic particles with enough energy to generate ionisation in the materials with which they interact are known as ionising radiation. Ionisation is the process by which a stable atom loses an electron (Chandra *et al.,* 2018; Powsner *et al*., 2006).

Ionising radiation was first understood in the early twentieth century by the significant contributions made by Wilhelm Roentgen, Henri Becquerel, and Marie and Pierre Curie. Roentgen observed a dye fluorescence outside an electric discharge tube coated in a black paper in 1985. Roentgen named those rays as x-rays. An Australian surgeon discovered a year later that this invisible energy may be utilised therapeutically to heal a hairy mole. In the same year, Becquerel discovered radioactivity when he exposed a shielded photographic plate to uranium salts. In 1989, Marie and Pierre curie discovered radioactive elements and introduced the term radioactivity to describe the properties of the discovered elements, such discoveries encouraged research work on radiation uses (Andreo *et al*., 2017).

In ionising radiation, the radiation takes the form of photons of electromagnetic energy and can be divided into two types, which are x-rays and gamma rays. Gamma rays are similar to x-rays with a key difference of how they are produced. X-rays are produced when electrons rearrange within an atom or when accelerated electrons strike a target whereas gamma rays originate from an excited nucleus of a radionuclide after it undergoes radioactive decay. In 1903, the British physicist Ernest Rutherford used the term gamma ray to describe the emissions of radioactive nuclei. Transition from a high energy level in the nucleus to a lower energy level results in emission of a photon to carry off the excess energy. The differences in the energy levels corresponds to photon wavelengths in the gamma ray region (Gupta, 2013).

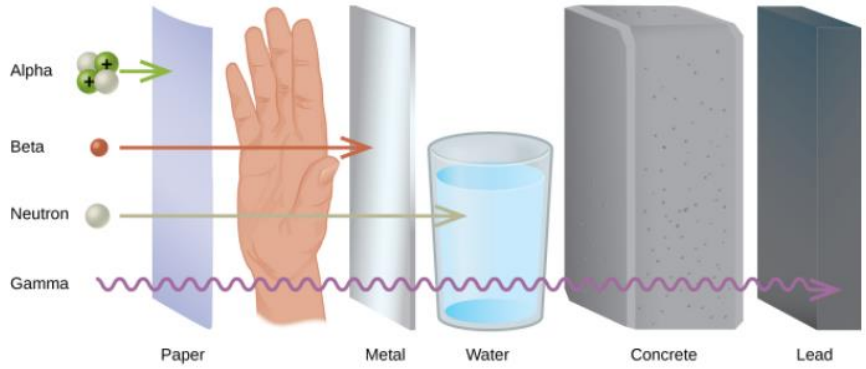

Figure 2.1 The ability of different types of radiation to pass through materials (Retrieved from https://opentextbc.ca/chemistry/chapter/21-6-biological-effects-of-radiation/ Data accessed May 2020).

2.2.1 Production of gamma rays

Gamma rays are ionising electromagnetic radiation obtained by the decay of an atomic nucleus or from positron annihilation with electrons. Gamma photons are the electromagnetic spectrum's most energetic photons (Patricelli *et al*., 2018). The photons resulting from deexcitation of nuclei have energies up to 20 MeV whereas those resulting from annihilations have much larger energies up to 150 MeV. In the

electromagnetic spectrum energy range, gamma rays have the high energy and short wavelength. Wavelength or frequency are considered as energy units for characterising radiation in the electromagnetic spectrum. Relationships between these quantities can be described by equations (1) and (2).

$$E=hxv \quad (1)$$

and

$$\lambda \times v=c \quad (2)$$

Where h (the Planck constant) = $4.135x10^{-15}$ eV Hz^{-1} and c (the velocity of light, or any electromagnetic radiation, in a vacuum) = $2.997926x10^{8}$ m s^{-1}.

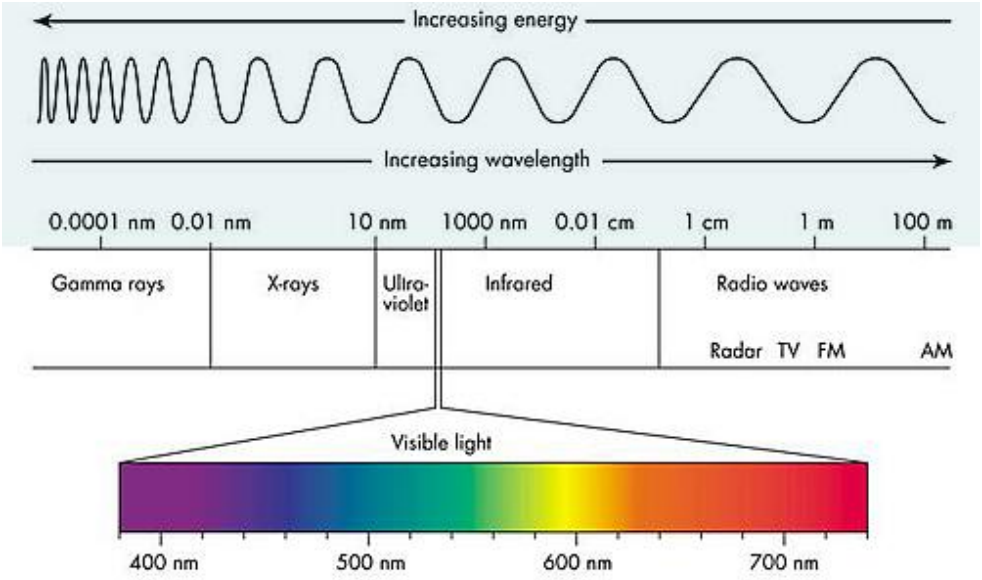

Figure 2.2 Electromagnetic spectrum (Retrieved from https://www.cyberphysics.co.uk/topics/light/emspect.htm Data accessed May 2020).

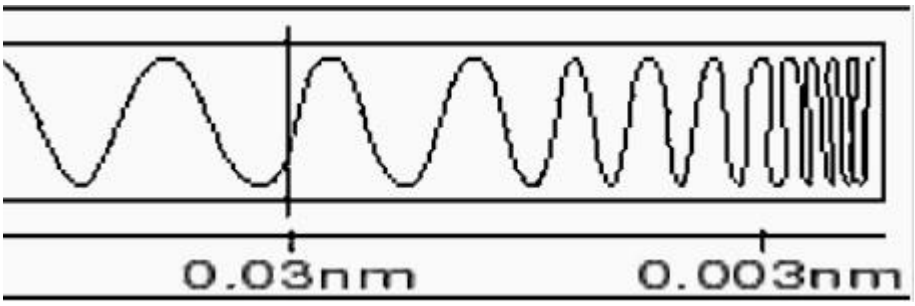

Figure 2.3 Gamma ray region of the electromagnetic spectrum (Retrieved from https://electromagneticspectrumscience.weebly.com/gamma-rays.html Data accessed May 2020).

Gamma rays can be produced in several ways, for instance during a collision with low energy photon when an electron transfer part of its energy to the photon results in a photon have an energy of 100 MeV, this known as inverse Compton scatter (Smith, 2020). When electron passing around a nucleus and got affected by its Colombian field, the electron slowed down and lost its energy in the form of gamma radiation, which known as bremsstrahlung or braking radiation (Aharonian, 2004).

Transitions between the least excited energy levels of a nucleus give rise to gamma radiation which refers to nucleus deexcitation which happens during specific thermonuclear interactions. Moreover, gamma rays can be produced in an extremely hot medium around ($T = 10^8$ K) called thermal radiation mechanism however this process mechanism is extremely rare and not fundamental to the production of gamma radiation. Thus, nonthermal processes are more common typical sources of gamma rays (Knödlseder, 2016). Gamma rays can be generated through physical processes, but this does not require the entire environment to be thermalised. Generally, all particles involved in an electromagnetic interaction accelerated through an external field, can be sources of gamma rays (Erramli *et al*, 2019).

2.3 Radiation interaction with matter

Gamma rays considered as ionising radiation that leads to the creation of radiation field when scattering by electrons and nuclei. Attenuation of gamma radiation occurs through the interaction of the gamma radiation with matter. Understanding gamma-ray detection and attenuation requires knowledge of gamma-ray interactions (Ragheb, 2011). Gamma rays fall in the range of 10 to 2000 keV and interact with absorbers by three major processes: photoelectric absorption, Compton scattering, and pair production. Gamma rays loses all of its energy, or part of its energy based on the interaction's possibility (Siegbahn, 2012).

Interaction of gamma photon with matter is a process with a broad spectrum of possible results, it might be absorbed or scattered and changing its direction with or without energy loss. The primary mechanism of energy deposition by photons in matter are photoelectric absorption, Compton scatter, and pair production.

2.3.1 Photoelectric effect

In a photoelectric process, a gamma photon interacts with an atom orbital electron, therefore losing all its energy and ceasing to be a gamma ray. One of the outer electrons fills the vacancy generated. In this case, the electron transition is accompanied by emission of very mild electromagnetic radiation. The gamma photon energy is split between the kinetic energy of the expelled electron and the characteristics transition radiation according to the energy conservation equation (3):

$$E_\gamma = E_e + E_a + E_B \tag{3}$$

where: E_γ is the initial gamma photon kinetic energy, E_e is the kinetic energy that the expelled electron has acquired, E_a is the recoiling atom's kinetic energy, E_B is the electron's binding energy in the atom equals the atom's excitation energy after electron ejection.

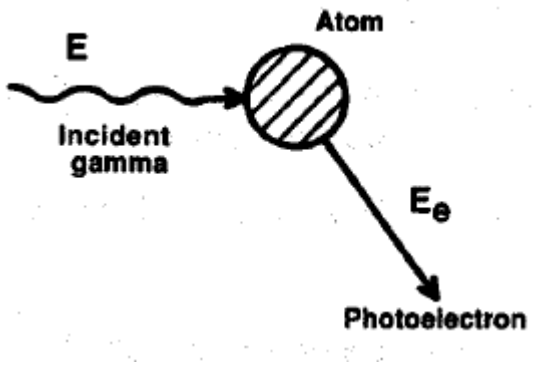

Figure 2.4 Schematic representation of the photoelectric absorption in process. (Retrieved from G. Nelson and D. Reilly, 1991).

The gamma ray energy, the electron binding energy, and the atomic number all influence the probability of photoelectric absorption. Photoelectrons are predominantly expelled from the K shell of an atom at gamma ray energy up to 0.5 MeV. The probability of photoelectric absorption increases rapidly as the gamma-ray energy decreases. For low-energy gamma rays, photoelectric absorption is the most common interaction.

Photoelectric absorption is critical for gamma ray detection because the gamma ray loses all of its energy, and the resultant pulse falls within the peak of the whole energy spectrum.

2.3.2 Compton scatter

Compton scattering is the most dominant process of gamma ray interaction with matter. It is the mechanism by which a gamma-photon interacts and transfers part of its energy to an outer weakly bonded electron. The electron loses its binding energy and becomes a free electron with a kinetic energy equal to the difference between the energy lost by the incident gamma photon and the energy gained by the electron. The kinetic energy of the scattered photon is nearly equal to the energy lost by the incident gamma photon as shown in equation (4).

$$E_e = E_\gamma - E' \quad (4)$$

where: E_e is the energy of scattered electron, E_γ is the energy of the incident gamma photon, E' is the energy of the scattered gamma photon.

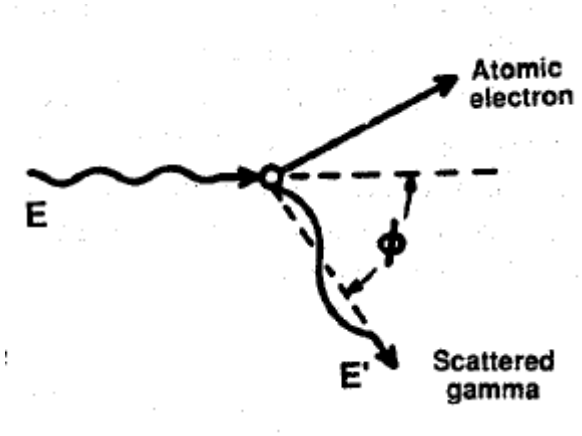

Figure 2.5 A schematic representation of Compton scattering (Retrieved from G. Nelson and D. Reilly, 1991).

2.3.3 Pair production

Pair production is a gamma ray interaction process that is possible to occur when the incident photon energy is above 1.02 MeV. Under the influence of a nucleus strong electromagnetic field, gamma ray photon can create an electron-positron pair. The minimum energy required to create electron-positron pair is their combined rest mass energy of 1.022 MeV. Therefore, for photon energies below this threshold, pair production cannot occur. However, when the photon energy exceeds this value, the excess energy appears as initial kinetic energy shared by the electron-positron pair. Both particles slow down and transfer their kinetic energy over an average distance of no more than a few millimetres.

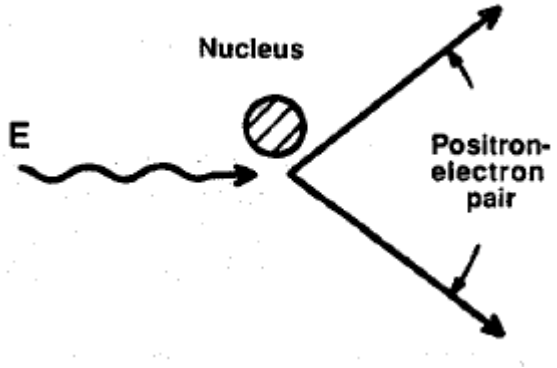

Figure 2.6 A schematic representation of pair production (Retrieved from G. Nelson and D. Reilly, 1991).

When the positively charged positron reaches the end of its track, it combines with an ordinary negatively charged electron from the absorber producing two annihilation photons in a process known as annihilation. Annihilation photons, like gamma rays, can travel long distances through matter without interacting.

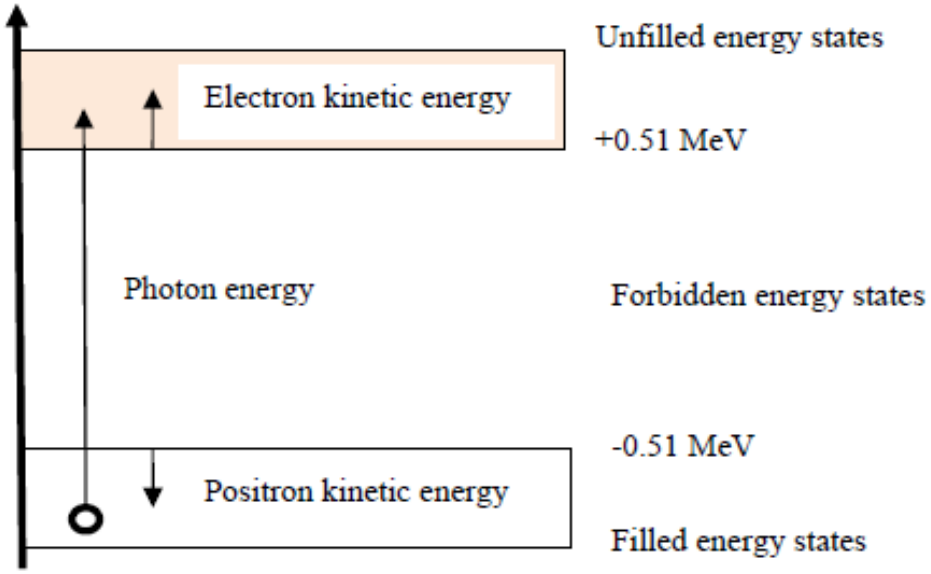

Figure 2.7 Formation of an electron-positron pair.

When the pair production occurs in a nuclear field, the photon energy hv is converted into 2mc^2 plus the kinetic energies T_+ and T_- of the electron-positron pair.

$$hv=2mc^2+T_{+}+T_{-} \quad (5)$$

The probability of these three interactions depends mainly on the incident gamma photon energy that passes through an object and the atomic number of the absorber. Firstly, the penetration of photons happens and it capable to transfer a portion of matter without any interaction. Second, it can interact with matter and be fully absorbed by depositing its energy and, eventually, it can interact and be distributed or deflected from its original path and deposit some of its energy (Maqbool, 2017).

Generally, the photoelectric effect prevails in low energy and dramatically increased in materials with a high atomic number. Therefore, high atomic elements are selected primarily for detectors used in gamma-ray energy measurements (Nambiar *et al*, 2012). For higher energies, pair production predominates and is often improved in high atomic number materials. There is a potential for an incident photon to induce several interactions in larger detectors, such as several consecutive Compton scattering, or pair production accompanied by the interaction of an annihilation photon. In radiation shielding practice, high atomic number materials served as good radiation shields to protect radiation workers and public from radiation shielding hazards.

2.4 Gamma ray attenuation

Gamma rays considered as the most penetrative among all types of radiations, they can never completely stop, but only attenuated. Based on the previous concept,

attenuation of gamma rays can be defined as the fraction of the transmitted rays that penetrate an absorber without interaction. The interaction between the incident gamma photon and absorber material of a specified thickness results in attenuation of the photon beam via absorption or scattering. The gradual decline in the photon beam intensity through absorbing medium is defined as attenuation. The photon beam's probability of penetrating absorbing material is represented by the attenuation coefficient for this material absorber. The more the gamma ray travel through the absorber, the more the interaction probability increases. If the intensity of the photon beam declines rapidly as it travels through a medium, this gives a high attenuation coefficient value (Attix, 2004). The attenuation coefficient is the sum of coefficient of different interaction modes, the photoelectric effect and Compton scatter. Radiation energy and the properties of the absorber control the proportion of each of these effects.

2.4.1 Linear attenuation coefficient

The linear attenuation and mass attenuation coefficients of components, molecules, and structures are frequently used in space physics, dosimetry, and plasma physics, as well as in the field of radiation physics, where they are also used to investigate the absorption of gamma radiation by a substance. They are also used in biological analysis, where gamma ray spectrometry is used to determine the activity concentration (Shaikh *et al*, 2020).

If a monoenergetic gamma rays collimated into a narrow beam and only those passed through an absorber material without any interaction detected by radiation detector, then the dependence should be simple exponential attenuation of gamma

rays. The exponential attenuation of the beam intensity is primarily determined by thickness, density, and atomic number of the material.

Linear attenuation factor (μ) is a constant that defines the fraction of the attenuated photons in a monoenergetic beam, per unit thickness of the material, and includes all interactions possible, including Compton scattering and photoelectric effect. Despite the fact that the linear attenuation coefficient is the most straightforward to calculate experimentally, it is not commonly computed for water, ice, and vapour due to its effect on the density of the absorbing material at any given energy, even though the same material is involved (Kurudirek, 2014).

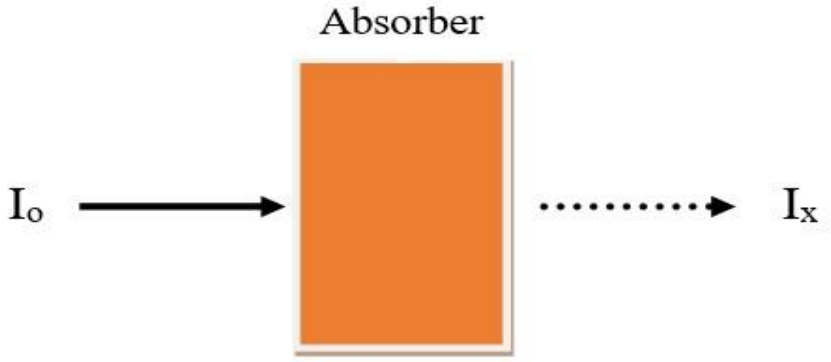

Figure 2.8 Transmission of gamma ray through absorber.

The photon intensity which passes through some matter, according to Lambert Beer's law, is provided by equation (6):

$$I = I_0 e^{-(\mu/\rho)\rho x} \tag{6}$$

In this equation, I represents photon attenuation intensity and I_0 is the intensity of the unattenuated photon. μ signify the linear attenuation coefficient, ρ is the material's mass density.

Generally, μ is affected by photon energy, atomic number (Z), and material thickness. Attenuation increases with lower photon energy, higher atomic number or thicker material (Powsner *et al*., 2013). In addition, the linear attenuation coefficient is the sum of individual (μ) of each material type due to the different types of photon beam interactions.

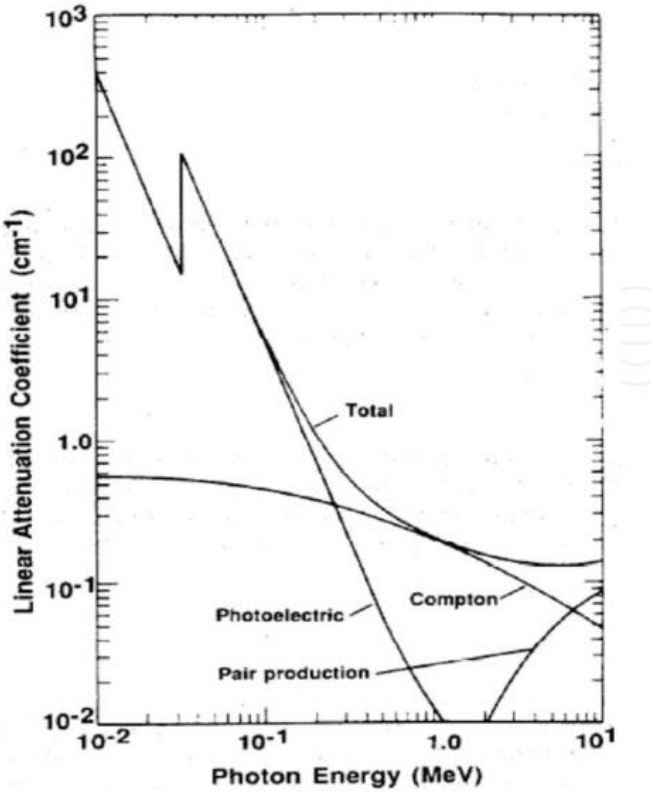

Figure 2.9 Linear attenuation coefficient of NaI showing contributions from photoelectric absorption, Compton scattering, and pair production (Retrieved from G. Nelson and D. Reilly, 1991).

2.4.2 Mass attenuation coefficient

The mass attenuation coefficient is a measurement of the overall interactions between incident photon and material in a given mass-per-unit area of material thickness. It is distinguished from the absorption coefficient, which is frequently smaller and measures the energy consumed by the medium (Gupta *et al*, 2014).